

**YIELD AND TRANSVERSE MOMENTUM OF RELATIVISTIC HYDROGEN ISOTOPES IN PHOTONUCLEAR SPALLATION OF  $^{32}\text{S}$  IONS AT 200A GeV****A. Abdelsalam<sup>a</sup>, S. Kamel<sup>1,b</sup>, Kh. Abdel-Waged<sup>c</sup>, N. Rashed<sup>d</sup>**<sup>a</sup>Physics Department, Faculty of Science, Cairo University, Cairo, Egypt<sup>b</sup>Physics Department, Faculty of Education, Ain Shams University, Cairo, Egypt<sup>c</sup>Physics Department, Faculty of Applied Science, UmmAl-Qura University, Makkah, Saudi Arabia<sup>d</sup>Physics Department, Faculty of Science, Cairo University, El Fayom Branch, Egypt

Received 21 November 2004, in final form 19 May 2005, accepted 20 May 2005

Production of multi-hydrogen ( $mH$ ) isotopes in the spallation of 200A GeV sulphur projectile using nuclear emulsion is reported. Yield of  $mH$  isotopes is studied and compared with that of the lowest energy (3.7A GeV) data. The two-source emission picture is used to describe the transverse momentum ( $P_T$ ) distribution of  $mH$  isotopes (with and without the effect of  $^{32}\text{S}$  ( $\gamma, p$ )  $^{31}\text{P}$  channel). The Rayleigh type  $P_T$ -distribution seems to be in agreement with the corresponding experimental data. The contributions of low and high temperature emission sources show a dependence on the photonuclear processes.

PACS: 25.75.-q, 25.70.Mn, 25.70.Pq

**1 Introduction**

Many experiments have been devoted to investigate the transverse momentum distribution ( $P_T$ ) of relativistic helium fragments using heavy ion beams when they became available at accelerators. The authors of references [1–4] investigated the  $P_T$  distribution of relativistic helium projectile fragments, produced in nucleus-emulsion collisions at 0.9 – 4.5A GeV/c. At high energy, such investigation has also been done [5] for relativistic He-fragments emerging from events having large impact parameters induced in the interactions of 200A GeV  $^{32}\text{S}$  ions with emulsion nuclei (Em). The investigations on the  $P_T$  distribution of relativistic He projectile fragments (PFs) show that there are two sources with different temperatures to emit relativistic helium fragments. These works are supported by Raha's arguments [6].

Recently, few similar experiments with relativistic proton PFs obtained either from nuclear [7–9] or electromagnetic [10, 11] events have already been carried out to study the  $P_T$  distribution. In the former case, Ghosh et al. [7, 8] reported  $P_T$  distributions of relativistic proton PFs emitting from the interactions of  $^{12}\text{C}$  and  $^{16}\text{O}$  with nuclear emulsion at 4.5 and 60A GeV/c, respectively. The comparison of these distributions with Maxwell-Boltzmann distribution gave the indication

---

<sup>1</sup>E-mail address: sayedks53@yahoo.com

of a single temperature in the fragmentation region. This is against the current explanations [1, 6], which favor of the existence of two different temperatures. The existing theories [1, 6] cannot account properly the single temperature emission of relativistic proton fragments [7, 8]. In addition, such observation does not agree with the results obtained by El- Nadi and co-workers [9] where there was an indication of two temperatures in the study of  $P_T$  distribution of relativistic proton PFs emitted from the inelastic interactions of  $^{32}\text{S}$  - Em at 3.7A GeV. In the case of electromagnetic dissociation (EMD) process, the author of Ref. 10 investigated the  $P_T$  distribution of only relativistic proton fragments produced in the dominant EMD process through the reactions  $^{32}\text{S} (\gamma, p) ^{31}\text{P}$  ( 92 relativistic proton PFs) and  $^{16}\text{O} (\gamma, p) ^{15}\text{N}$  ( 45 relativistic proton PFs) at 200A GeV. The obtained  $P_T$  distribution in each reaction is fitted by a double Rayleigh distribution having two different temperatures. This two-temperature structure of relativistic single charged fragments is described in Ref. 11 by a simple model based on a two-source emission picture.

In the present work and owing to the collection of our exclusive data given in Ref. 12, it was possible to do further study of  $P_T$  distribution of all relativistic single charged particles (308 hydrogen isotopes) emitted in the different visible decay modes (i.e. those involving charged fragments) of  $^{32}\text{S}$  spallation at 200A GeV. Consequently, the given H-particles  $P_T$ -distribution analyzed with and without the effect of single proton production through the  $^{32}\text{S} (\gamma, p) ^{31}\text{P}$  channel [10], the dominant mode of decay (44 %), within a two-source emission formalism [11].

## 2 Experimental details

In the present work, a stack of Fuji emulsion plates was exposed horizontally to the 200A GeV  $^{32}\text{S}$  ions at the CERN-SPS (Exp. No. EMUO3). To obtain high scanning efficiency, the pellicles were scanned under  $100 \times$  magnification by doubly scanning along the beam tracks, fast in the forward direction and slow in the backward one. The beam tracks were picked up at a distance of 4 mm from the entrance edge, and within the central 80% of the pellicle thickness. Each beam track was carefully followed up to a distance of 5 cm or until the point of interaction with an emulsion nucleus. Other details concerning the chemical composition of the emulsion used, irradiation and scanning are given in Refs. 12 and 13. In each event, the following visual features were recorded:  $N_b$ , the number of black tracks;  $N_g$ , the number of grey tracks;  $N_h = N_b + N_g$ , the number of heavy tracks from the target nucleus;  $N_s$ , the number of minimum ionizing shower tracks;  $N_H$ , the number of H-particles of charge  $Z = 1$ ;  $N_Z$ , the number of PFs of charge  $Z \geq 2$ . H-particles and PFs are produced within the fragmentation cone defined by  $\theta \leq \theta_c = P_f/P_{\text{beam}}$ , where  $P_f$  is the Fermi momentum, estimated to be  $\approx 200$  MeV/c ( $\theta_c \approx 1$  mrad at 200A GeV). Each event was carefully examined and qualitatively classified into three principal categories: (i) central, (ii) peripheral and (iii) electromagnetic events.

The pure EMD events are then selected to be analyzed. These events generated by the EMD of the projectile nucleus are generated in collisions involving impact parameters large enough so that no nuclear interactions occur. Extremely strong electromagnetic fields from heavy nuclei are produced for a very short time at the projectile; such events typically consist of projectile fragments, which proceed essentially in the direction of the projectile nucleus. The present candidate EMD events were selected [14, 15] with no visible target excitation ( $N_h = 0$ ) or secondary particle production ( $N_s = 0$ ) together with the condition that the sum of measured

charges of all the outgoing fragments ( $Z \geq 1$ ) inside the fragmentation cone must equal the charge of the incident  $^{32}\text{S}$  beam. Exclusion of low-energy  $e^+e^-$  pairs, high-energy  $\gamma$ -rays and elastic scattering events was done [14, 16]. Upon application of these stringent selection criteria, 210 EMD events out of 1459 observed events were determined to be due to the clean breakup of the  $^{32}\text{S}$  projectile. Charge measurements were performed on projectile EMD fragments by  $\delta$ -ray counting. For light fragments ( $Z = 2 - 4$ ), complementary gap counting was undertaken [17]. In general, the detection of  $Z \leq 2$  PFs is quite definite due to their distinctive grain density and the use of electron sensitive Fuji nuclear emulsion detectors allows an exclusive type of analysis on an event-by-event basis. It is well known that the emulsion detector covers a  $4\pi$  geometry and has a very high spatial resolution. The latter feature is very helpful in identifying and measuring the angles of individual PFs formed in EMD events, even when the fragmentation cone of the PFs is very narrow.

The emission angles of all PFs in EMD events of 200A GeV  $^{32}\text{S}$  projectile were determined from the vector directions of the incident beam and emitted fragments following Ref. 15. The accuracy in the angular measurements in the emulsion is higher than 0.1 mrad for angles  $\theta \leq 1$  mrad. In nuclear emulsion experiment, the (pseudo) transverse momentum of the projectile fragment can be obtained from the emission angle measurement [9]. Since we are concerned with the relativistic hydrogen particles in the break up modes of  $^{32}\text{S}$  ions at 200A GeV, the transverse momentum  $P_T$  of H-particles can be determined with the assumption that the hydrogen isotopes have the same longitudinal velocity as that of the incident  $^{32}\text{S}$  beam.

### 3 Results

With the successful acceleration of heavy nuclei to ultra-relativistic energies, the study of EMD in nuclear emulsion offers a number of experimental advantages particularly in the identification of specific final states. Since in the emulsion experiment, only charged particles can be identified such that the charge of each but not the mass could be determined, neutrons cannot be detected and isotopes are not separated. Consequently, in this work, the fragmentation modes having fragments accompanied with one or more neutrons are misidentified.

In Table 1, we report the detected 210 EMD events due to the clean break up of 200A GeV  $^{32}\text{S}$  projectile in emulsion. One can see that the present events are observed in only 28 channels (different visible decay modes) ordered according to  $Z_{\text{max}}$ , the charge of the heaviest PF emitted in an event. At the beginning, one can observe the simple photonuclear process in which one or two light PFs dissociated from the projectile nucleus leaving the residual nucleus, which cools down, forming a heavy fragment. It is possible to think that this process is characterized by low temperature. On the other hand, at the end of the table one can notice a hard photonuclear process in which the sulphur nucleus has been decayed into H and He fragments.

In Fig. 1, we show the charge yield curve for  $^{32}\text{S}$  spallation in the emulsion at two widely different energies. The solid histogram in Fig. 1 represents our data at 200A GeV while the dashed one represents the data of 3.7A GeV [12]. The two distributions have a characteristic U-shaped form. The figure shows clearly the effect of incident energy at large values of  $Z$ , i.e. at  $Z \geq 10$ . The number of single charged particles,  $N_H$ , could characterize the degree of hardness of interaction. These particles may be emitted from different sources. Therefore, for better probing the dynamics of heavy ion reactions, the present work which is an extension to

Tab. 1. Different visible decay modes of  $^{32}\text{S}$ -spallation at 200A GeV and the corresponding number of events.

Decay mode	No. of events	Decay mode	No. of events
$^{31}\text{P} + p$	92	$^{19}\text{F} + 2\text{He} + 3\text{H}$	1
$^{28}\text{Si} + \text{He}$	30	$^{19}\text{F} + 3\text{He} + \text{H}$	2
$^{28}\text{Si} + 2\text{H}$	20	$^{16}\text{O} + 3\text{He} + 2\text{H}$	1
$^{27}\text{Al} + \text{He} + \text{H}$	15	$^{16}\text{O} + 2\text{He} + 4\text{H}$	1
$^{27}\text{Al} + 3\text{H}$	6	$^{14}\text{N} + 3\text{He} + 3\text{H}$	1
$^{24}\text{Mg} + 2\text{He}$	5	$^{14}\text{N} + 2\text{He} + 5\text{H}$	1
$^{24}\text{Mg} + \text{He} + 2\text{H}$	4	$^{12}\text{C} + 3\text{He} + 4\text{H}$	1
$^{24}\text{Mg} + 4\text{H}$	5	$^{11}\text{B} + 4\text{He} + 3\text{H}$	1
$^{23}\text{Na} + 2\text{He} + \text{H}$	4	$^{11}\text{B} + 2\text{He} + 7\text{H}$	1
$^{23}\text{Na} + ^7\text{Li} + 2\text{H}$	1	$^9\text{Be} + 2\text{He} + 8\text{H}$	1
$^{23}\text{Na} + \text{He} + 3\text{H}$	4	$^7\text{Li} + 4\text{He} + 5\text{H}$	1
$^{23}\text{Na} + 5\text{H}$	3	$6\text{He} + 4\text{H}$	1
$^{20}\text{Ne} + 2\text{He} + 2\text{H}$	3	$5\text{He} + 6\text{H}$	1
$^{20}\text{Ne} + \text{He} + 4\text{H}$	3	$4\text{He} + 8\text{H}$	1

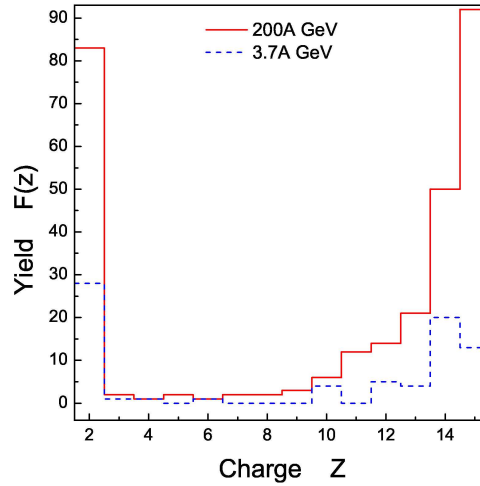


Fig. 1. The charge yield curve of the PFs emitted in the EMD events for the present  $^{32}\text{S}$  projectile at 200A GeV (the solid histogram) and 3.7A GeV [12] (the dashed histogram).

our previous one [10], deals only with a sub sample of 175 EMD events having one or more H-particles in the final state (in addition to the heavy fragments), see Table 1. Following the analysis of the angular distribution of 308 H-particles presented in our sub sample, the average values of emission angles,  $\langle\theta_H\rangle$ , are found [10] to be  $(0.889 \pm 0.081)$  mrad.

Tab. 2. Relative rates (in percentage) of visible channels of multi-hydrogen (mH) isotopes together with that of the single proton.

Multiplicity	No. of tracks	Relative rates (%)
1p	92	43.8
1H	113	53.8
2H	58	13.8
3H	39	6.2
4H	44	5.2
5H	25	2.4
6H	6	0.5
7H	7	0.5
8H	16	1.0

In fact, we deal with the interested EMD data sub sample as two major parts, namely single charged particles [10] (mostly are protons) which are the most abundant particle in Table 1,  $^{32}\text{S}(\gamma, p)$   $^{31}\text{P}$ , and the multiple hydrogen isotopes, mH. The measured cross section in Ref. 12 for the former decay mode,  $\sigma_{\text{EMD}}^{\text{p}}$  equals to  $(502 \pm 52)$  mb which represents  $(33 \pm 3)$  % of the measured total EMD cross section [12] where,  $\sigma_{\text{EMD}}^{\text{tot.}} = (1531 \pm 103)$  mb. While for the later ones, the cross section measured for mH emission channels,  $\sigma_{\text{EMD}}^{\text{mH}}$  represent about  $(55 \pm 4)$  % of the measured total EMD cross section. The cross sections measured for 1p and 1H, 2H,...,mH emission channels induced by Ag target in emulsion [18, 19], see after, sum to about  $(1340 \pm 90)$  mb, which represent roughly 88% of the  $\sigma_{\text{EMD}}^{\text{tot.}}$ . This permits a comparison between  $P_T$  distributions of these two major parts. This study is considered complementary to energy measurements already reported in our recent work [18]. All of this information could help to obtain a consistent picture of the entire reaction process.

In Table 2, we show the production relative rates (in percentage) of visible channels for the multi-hydrogen isotopes (mH) together with that for a single proton (1p). The latter reaction channel  $^{32}\text{S}(\gamma, p)$   $^{31}\text{P}$  at 200A GeV has been studied in Ref. 10, reporting that the majority of events in this dominant channel may be attributed to the absorption of giant dipole resonances (GDRs). On the other hand, one can notice from Table 2 that the behavior of decreasing yield and the extension of the production probability to higher multiplicity values of  $N_H$  (up to 8) may reflect the dependence of the degree of break-up on the response of projectile nucleus to the absorption of one or more than one virtual photon, i.e. several simultaneous GDR photons [18, 20].

Our total EMD cross section measured by the interaction of  $^{32}\text{S}$  in an Ag target is  $(1531 \pm 103)$  mb. This value is computed using the relation [18, 19]  $\sigma = f/\rho\lambda$ , where  $\rho$  is the concentration of Ag nuclei in the emulsion used ( $\rho = 1.01 \times 10^{22}$  atoms/cm<sup>3</sup>) and  $f$  is the weight factor of Ag nuclei ( $f = 0.62$ ). From the Weizsacker-Williams (WW) calculation [21], the total integrated EMD cross section is estimated to be  $(1869 \pm 100)$  mb (using the measured  $\sigma(\gamma, \text{tot})$  total photon absorption cross section [22]) which is significantly higher than our measurements. However, a closer agreement with our data is obtained if we subtract the one-neutron (1n) contribution (281 mb) (calculated by the WW using the measured  $\sigma(\gamma, n)$  [22]) from the WW total EMD cross

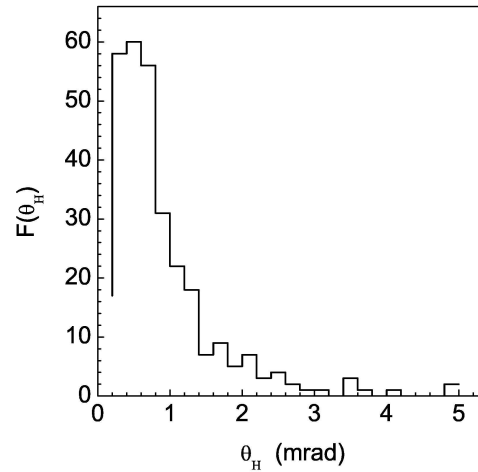


Fig. 2. The measured angular distribution for all  $Z = 1$  particles emitted in the total sample (210 detected EMD events) of  $^{32}\text{S}$  break-up at 200A GeV.

section.

In Fig. 2, we show the angular distribution measured for all  $Z = 1$  particles in the sub sample (175 EMD events) with an average emission angle  $\langle \theta_H \rangle = 0.89 \pm 0.08$  mrad. This figure shows that the peak is broader and the tail becomes larger i.e. there are few H-isotopes emitted with angles greater than the critical fragmentation cone ( $\theta_c$ ).

In the following, the investigations on the transverse momentum distribution of the present relativistic H-particles will occur using the model of Ref. 11 introducing a two-source emission picture to describe such  $P_T$  distribution. The description of this model [11, 23] is summarized below.

In the EMD process, the local region of the colliding nucleus obtained the virtual photon energies from the collisions. Then the local region has some excitation energy and remains in a high excitation state. A small part of the excitation energy of the local region is transmitted to the other part of the colliding nucleus. Then the other part remains in a low excitation state. The completely colliding nucleus does not remain in the equilibrium state, but the local region excited by virtual photon energies and the other part of the colliding nucleus remain in the local equilibrium state. The whole nucleus acts coherently, but each nucleon does not directly obtain the virtual photon energies. The nuclei in EMD process are thus excited non-evenly. The author [23] treated the nucleus as a physical object with given volume. For the EMD process, the two sources are the nuclear local region (hot source) excited by virtual photon energies and the other part (cold source).

According to this picture [11, 24], two emission sources having different temperatures exist and may remain in different excitation energies. In the rest frame of the emission source, it is assumed that the three particle momentum components obey a Gaussian distribution having the standard deviation ( $\sigma_i$ ) with the same width.

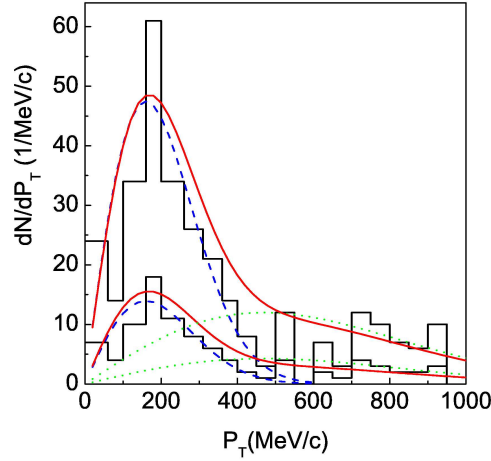


Fig. 3. The  $P_T$  distribution for all (308)  $H$  - particles (thick lines), i.e. with the effect of  $p + {}^{31}P$  channel, in comparison with that of 92 protons (thin lines). The solid histograms are the present experimental data. The curves (see the text) are our calculated results.

The transverse momentum  $P_T$  ( $= \sqrt{P_x^2 + P_y^2}$ ) obeys the Rayleigh distribution [24]:

$$f_{P_T}(P_T, \sigma_i) = \frac{P_T}{\sigma_i^2} \exp\left(\frac{-P_T^2}{2\sigma_i^2}\right). \quad (1)$$

For a two-source emission process, the  $P_T$  distribution is the sum of two Rayleigh distributions:

$$f_{P_T}(P_T) = A_L f(P_T, \sigma_L) + A_H f(P_T, \sigma_H), \quad (2)$$

where  $A_L$  and  $A_H$  are the normalization factors for the low and high temperature emission of mH particles, respectively, while  $\sigma_L$  and  $\sigma_H$  are related to the temperature  $T$  of the emission sources [23] according to the relation  $\sigma^2 = m_0 \gamma T$  ( $\gamma$  is the mean Lorentz factor).

In this work, the transverse momentum of all (308)  $H$  particles emitted in the 200A GeV  ${}^{32}S$  break-up is calculated. We divided such particles into two groups, as we already mentioned. The first group contains 92 protons emitted in the dominant decay mode  ${}^{32}S(\gamma, p){}^{31}P$  and the second one contains 216  $H$  particles emitted in the different other decay modes of Table 1. Therefore, the transverse momentum distributions are investigated in Figs. 3 and 4 with and without the effect of protons produced in the  $p + {}^{31}P$  channel, respectively.

In Fig. 3, the  $P_T$  distribution for all  $H$  particles is compared with the corresponding one of 92 protons. The solid histograms are the present experimental data. The curves are our calculated results. The contributions of low and high temperature emission sources are given by the dotted and dashed curves, respectively. The solid curves are the sum of the dotted and dashed curves. The values  $\sigma_L$  and  $\sigma_H$  are obtained by fitting the experimental data and equal 160 MeV/c and 470 MeV/c, respectively. The values of  $\chi^2/\text{degrees of freedom (DOF)}$  for the low and high components of all mH isotopes are 0.507 and 1.319, respectively. While for the single protons, the corresponding values are 0.491 and 1.861, respectively.

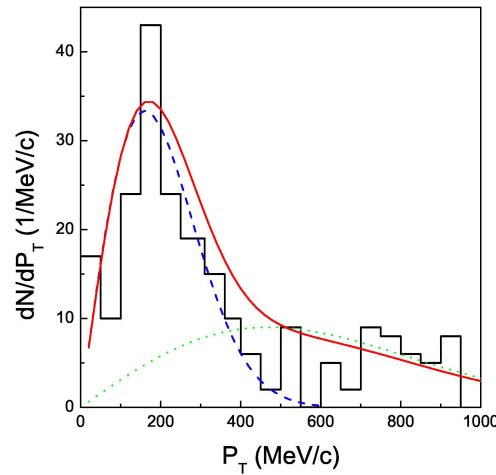


Fig. 4. The same as Fig. 3 but for only 216  $H$  - particles i.e. without the effect of  $p + {}^{31}\text{P}$  channel.

In Fig. 4, we show the  $P_T$  distribution for the 216  $H$  particles i.e. without the effect of  $p + {}^{31}\text{P}$  channel. The other conditions are the same as Fig. 3. The values of  $\chi^2/\text{DOF}$  are now 0.518 and 1.857, respectively.

From Figs. 3 and 4, one can see that the three experimental distributions have the same shape and the same trend. The best fit is observed for the low components of the  $P_T$  distributions, where the minimum value of  $\chi^2/\text{DOF}$  is obtained. We also notice that the two-source emission picture gives a good description of the transverse momentum distribution for  $H$  particles in both investigated cases, i.e. with and without the effect of  $p + {}^{31}\text{P}$  channel. This description shows the dependence of shape of  $P_T$ -distribution on the contributions of low and high temperature emission sources such that the great difference in these contributions cannot be described by a single temperature.

#### 4 Conclusions

A study has been made of the production of multi-hydrogen (mH) isotopes during the break-up of 200A GeV  ${}^{32}\text{S}$  projectile in nuclear emulsion. The decreasing yield and the extension of the production probability to higher multiplicity values may reflect the dependence of the degree of break-up on the response of the projectile nucleus to the absorption of one or more than one virtual photon. The  $P_T$ -distribution of mH isotopes was analyzed with and without the effect of single proton production through the  ${}^{32}\text{S}(\gamma, p){}^{31}\text{P}$  channel, the dominant mode of decay (44%), within a two-source emission formalism. The calculated results show a good agreement with the experimental data. Although the  $P_T$ -distributions appear no evidence for the effect of single proton channel, the contributions of low and high temperature emission sources seem to depend on the degree of photonuclear (simple or hard) processes. That is the process leading to higher temperature will lead to the emission of multi-particles of hydrogen isotopes in the final state. This may be explained, based on the energy spread shown in Ref. 18, in terms of multiphoton



absorption, i.e. absorption of several simultaneous GDR photons.

**Acknowledgement:** This work was carried out at Mohamed El-Nadi High Energy Lab., Faculty of Science, Cairo University. The authors appreciate very much the help of the authorities of CERN SPS with the irradiation of the plates.

#### References

- [1] K. B. Bhalla, M. Chaudhry, S. Lokanathan et al.: *Nucl. Phys. A* **367** (1981) 446
- [2] H. G. Baumgardt, E. M. Friedlander, E. Schopper: *J. Phys. G: Nucl. Phys.* **7** (1981) L175
- [3] M. M. Aggarwal, K. B. Bhalla, G. Das, P. L. Jain: *Phys. Rev. C* **27** (1983) 640
- [4] D. Ghosh, J. Roy, R. Sengupta: *J. Phys. G* **14** (1988) 711
- [5] S. Kamel: *Il Nuovo Cimento A* **112** (1999) 733
- [6] S. Raha, R. M. Weiner, J. W. Wheeler: *Phys. Rev. Lett.* **53** (1984) 138
- [7] D. Ghosh, J. Roy, S. Sarkar: *Nuovo Cimento Soc. Ital. Fiz. A* **103** (1990) 423
- [8] D. Ghosh, S. K. Das, K. Ghosh: *Nuovo Cimento Soc. Ital. Fiz. A* **110** (1997) 565
- [9] M. El-Nadi, A. Abdelsalam, A. Hussien et al.: *Radiat. Meas.* **28** (1997) 231
- [10] S. Kamel: *Nuovo Cimento Soc. Ital. Fiz. A* **112** (1999) 327
- [11] Fu-Hu Liu: *Chin. J. Phys.* **40** (2002) 12
- [12] M. El-Nadi, A. Abdelsalam, A. Hussien, E. A. Shaat, N. Ali- Mossa, Z. Abou Moussa, S. Kamel, Kh. Abdel-Waged, M. E. Hafiz: *J. Phys. G: Nucl. Part. Phys.* **28** (2002) 241
- [13] M. El-Nadi, A. Abdelsalam, A. Hussien, E. A. Shaat, N. Ali- Mossa, Z. Abou Moussa, S. Kamel, Kh. Abdel- Waged, E. El-Falaky: *Int. J. Mod. Phys. E* **6** (1997) 191
- [14] G. Baroni V. Bisi, A.C. Breslin et al.: *Nucl. Phys. A* **516** (1990) 673
- [15] G. Singh, K. Sengupt, P. L. Jain: *Phys. Rev. C* **41** (1990) 999
- [16] S. Kamel: *Phys. Lett. B* **368** (1996) 291
- [17] P. L. Jain, M. M. Aggarwal, K. L. Gomber: *Phys. Rev. C* **34** (1986) 726
- [18] M. El-Nadi, A. Abdelsalam, E. A. Shaat, N. Ali- Mossa , Z. Abou Moussa, S. Kamel, N. Rashed, W. Osman, M. E. Hafiz: *Can. J. Phys.* **82** (2004) 263
- [19] G. Singh, P. L. Jain: *Z. Phys. A* **344** (1992) 73
- [20] J. Barrette, R. Bellwied, P. Braun-Munzinger et al.: *Phys. Rev. C* **51** (1995) 865 ; W. J. Llope, P. Braun-Munzinger: *Phys. Rev. C* **41** (1990) 2644
- [21] E. Fermi: *Z. Phys.* **29** (1924) 315 ; C. F. Weizacker: *ibid.* **88** (1934) 612 ; E. J. Williams: *Phys. Rev.* **45** (1934) 729
- [22] C. B. Brechtmann, W. Heinrich: *Z. Phys. A* **330** (1988) 407 and *ibid.* **331** (1988) 463
- [23] Fu-Hu-Liu, Yuri A. Panebratsev: *Phys. Rev. C* **59** (1999) 941 ; Fu-Hu-Liu: *Chin. J. Phys.* **39** (2001) 401
- [24] U. A. Abdurazakova, L. E. Bengus, A. I. Bondarenko, R. U. Kholmatova, G. M. Chernov: *Sov. J. Nucl. Phys.* **47** (1988) 827